# Highly Dynamic AC Current Control for Modular Multilevel Converters

D. Braeckle ⓘ, P. Himmelmann ⓘ, S. Mersche ⓘ, L. Stefanski ⓘ, M. Hiller ⓘ
Karlsruhe Institute of Technology
Karlsruhe, Germany
Phone: +49 (721) 608-42922
Email: dennis.braeckle@kit.edu
URL: https://eti.kit.edu

## Keywords

## Abstract

A highly robust and dynamic control of the MMC grid currents is necessary to ensure grid stability. Based on a state space modelling of the MMC, a real time capable indirect modelbased control is presented. Measurements with a laboratory setup show the reliability even under disturbed grid conditions.

## Introduction

The MMC as shown in Fig. 1 is a topology which was presented in 2002 [1] and has since become established as the system of choice when it comes to the transmission of large amounts of power over long distances [2]. The development of multilevel converters enables the continuing development of larger high and extra-high voltage grids, both AC grids and DC grids [3–5]. In addition to transporting large amounts of electrical energy, modular multilevel converters are also used as components to improve the quality of the grid voltage. They support the grid asflexible AC transmissionsystems (FACTS) or static synchronous compensator (STATCOM) by making use of the existing line capacities and by providing reactive power [6, 7]. The topology is also considered promising for use as DC breakers in extensive DC networks [8, 9] or for use as galvanic isolation [10]. The MMC is also becoming increasingly popular as drive converter [11, 12].

If the MMC is used as a grid-side power converter, the grid-side control in stationary operation and in case of a fault must be considered in detail. An indirect model-based predictive control (MPC) approach of the AC side is proposed, which in connection with the modeling also allows a safe operation in case of grid failure. Due to the highly accurate feedforward control of the AC voltage, the use of a PI current controller in rotating coordinates according to the state of the art is conceivable. However, it is not possible to control constant power or sinusoidal currents even in the event of a fault without considerable additional effort. An MPC allows a trajectory-based control of the AC currents [13]. The MPC can basically be divided into two categories for power electronic systems. The direct predictive control directly optimizes the switching times of the power semiconductors under consideration of the boundary conditions [14–16]. It has the disadvantage, that the complexity of the calculation increases with the number of switches or cells in the converter, since the switching times are calculated directly. For the later implementation a control frequency of at least $f = 8\,\text{kHz}$ is aimed at. The optimization associated with the MPC must be calculated in the available control time to satisfy the real-time condition. Therefore, the MPC is used exclusively for the control of the AC currents.
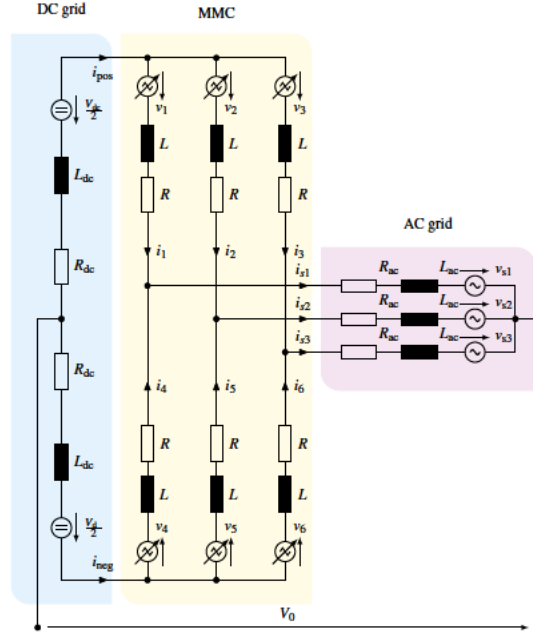
Fig. 1: Circuit diagram of the MMC

The paper is organized as follows. First, the system equations for the MMC system are derived and decoupled shortly. Secondly, the fundamentals and the design of the indirect MPC are given. Equations for the AC side control of the MMC are derived. Subsequently, the laboratory setup is presented to implement the MPC approach. Last, measurement results are shown to verify the control approach. Conclusions follow.

## Fundamentals

### MMC System Equations

The system equations of the MMC are well known (e.g. [11]). A representation using the state space notation allows to perform a simple similarity transform to decouple the system as shown in [17]. The result are decoupled system matrices in transformed coordinates as basis for further design of the control algorithms. In the following, a tilde ˜ denotes a representation in transformed coordinates. The similarity transform is applied to the system equations of the MMC

$$\frac{\mathrm{d}}{\mathrm{d}t}\tilde{\underline{i}} = TAT^{\top}\tilde{\underline{i}} + TB\underline{\tilde{v}} + TF\underline{z}. \tag{1a}$$

which results with the input transformation $\underline{\tilde{v}} = T\underline{v}$ in

$$\frac{\mathrm{d}}{\mathrm{d}t}\tilde{\underline{i}} = \tilde{\underline{A}}\tilde{\underline{i}} + \tilde{\underline{B}}\underline{\tilde{v}} + \tilde{\underline{F}}\underline{z}$$

$$= -\begin{bmatrix} 0 & 0 & 0 & 0 & 0 & 0 \\ 0 & \frac{\tilde{R}_2}{L_2} & 0 & 0 & 0 & 0 \\ 0 & 0 & \frac{\tilde{R}_3}{L_3} & 0 & 0 & 0 \\ 0 & 0 & 0 & \frac{\tilde{R}_4}{L_4} & 0 & 0 \\ 0 & 0 & 0 & 0 & \frac{\tilde{R}_5}{L_5} & 0 \\ 0 & 0 & 0 & 0 & 0 & \frac{\tilde{R}_6}{L_6} \end{bmatrix}\tilde{\underline{i}} - \begin{bmatrix} 0 & 0 & 0 & 0 & 0 & 0 \\ 0 & \frac{1}{L_2} & 0 & 0 & 0 & 0 \\ 0 & 0 & \frac{1}{L_3} & 0 & 0 & 0 \\ 0 & 0 & 0 & \frac{1}{L_4} & 0 & 0 \\ 0 & 0 & 0 & 0 & \frac{1}{L_5} & 0 \\ 0 & 0 & 0 & 0 & 0 & \frac{1}{L_6} \end{bmatrix}\underline{\tilde{v}} + \begin{bmatrix} 0 & 0 & 0 & 0 \\ 0 & 0 & 0 & -\frac{\sqrt{6}}{3L_2} \\ 0 & 0 & 0 & 0 \\ 0 & 0 & 0 & 0 \\ \frac{1}{L_5} & -\frac{1}{L_5} & 0 & 0 \\ \frac{\sqrt{3}}{3L_5} & \frac{\sqrt{3}}{3L_5} & -\frac{2\sqrt{3}}{3L_6} & 0 \end{bmatrix}\underline{z} \tag{1b}$$

$$\underline{w} = T^{\top}\tilde{\underline{i}} \odot T^{\top}\underline{\tilde{v}} \tag{1c}$$

(a) Line 1: Zero sequence voltage

(b) Line 2: DC side

(c) Lines 3 and 4: Internal currents
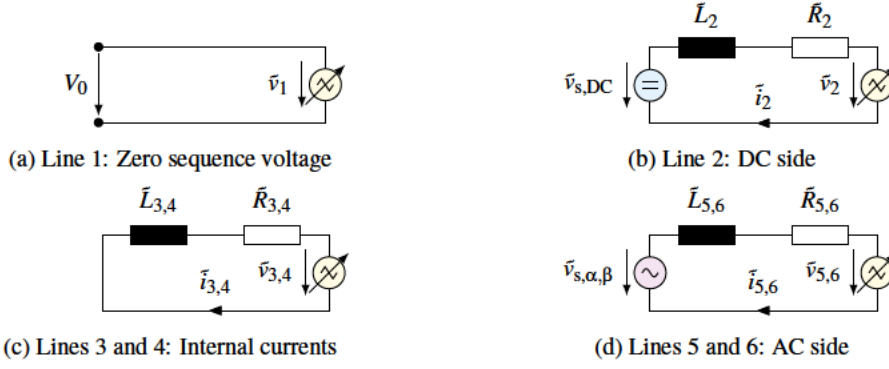
(d) Lines 5 and 6: AC side

Fig. 2: Decoupled representation of the MMC

With $\underline{z} = [v_{s1}, v_{s2}, v_{s3}, V_{DC}]^\top$ and $\odot$ describes the element wise multiplication of the respective entries. $T$ is the transformation matrix determined according to [17]

$$T = \begin{bmatrix} \frac{1}{\sqrt{6}} & \frac{1}{\sqrt{6}} & \frac{1}{\sqrt{6}} & \frac{1}{\sqrt{6}} & \frac{1}{\sqrt{6}} & \frac{1}{\sqrt{6}} \\ -\frac{1}{\sqrt{6}} & -\frac{1}{\sqrt{6}} & -\frac{1}{\sqrt{6}} & \frac{1}{\sqrt{6}} & \frac{1}{\sqrt{6}} & \frac{1}{\sqrt{6}} \\ \frac{1}{2} & -\frac{1}{2} & 0 & -\frac{1}{2} & \frac{1}{2} & 0 \\ \frac{1}{\sqrt{12}} & \frac{1}{\sqrt{12}} & -\frac{1}{\sqrt{3}} & \frac{1}{\sqrt{12}} & \frac{1}{\sqrt{12}} & -\frac{1}{\sqrt{3}} \\ -\frac{1}{2} & \frac{1}{2} & 0 & -\frac{1}{2} & \frac{1}{2} & 0 \\ -\frac{1}{\sqrt{12}} & -\frac{1}{\sqrt{12}} & \frac{1}{\sqrt{3}} & -\frac{1}{\sqrt{12}} & -\frac{1}{\sqrt{12}} & \frac{1}{\sqrt{3}} \end{bmatrix} \tag{1d}$$

The matrices $\tilde{\underline{A}}$, $\tilde{\underline{B}}$, $\tilde{\underline{F}}$ and $\tilde{\underline{C}}$ describe the MMC in transformed coordinates. These matrices are diagonal matrices except $\tilde{\underline{F}}$. Therefore, the transformed currents of the system are decoupled.

$\tilde{\underline{A}}$ depends on the branch inductance $\check{L}$ and the resistance $\check{R}$. In addition, the DC side inductance and resistance as well as the AC side parameters and influence the system matrix. $\tilde{\underline{B}}$ and $\tilde{\underline{F}}$ only depend on the inductances $\check{L}$. The MMC is described completely by those relations.

For this paper it is assumed, that all currents and energies are controlled to their setpoints using a cascaded control approach [11, 17]. Figure 2(d) represents the 5th and 6th line of the system equations (1b). This is the decoupled AC side of the MMC and will be controlled by a model-based predictive control approach.

## Fundamentals and Design of the Mpdel Based Predictive Control Approach

A dynamic, state-space model of the system predicts its further development over a given prediction horizon. Boundary conditions are considered and the optimal trajectories of the output variables are determined by solving a mathematical optimization problem. The formulation of a suitable optimization function is one of the biggest challenges in an MPC approach. In addition, the optimization has to take place in real time. This places demands on the optimization equation as its solution must not be overly complicated to calculate.

The state space model is the basis of the control. The constraints of the input, output and state variables are directly considered in the controller design. The cost function describes the control objective. It includes, for example, deviations from the reference value or the effort to achieve the control objective. The optimization then minimizes the cost function taking into account the model and the constraints. The prediction horizon is recalculated for each time step but only the first step is realized. A feedback is obtained considering new measured values and hence robustness of the controller in each time instant. Based on the state space representation of the MMC in (1b) and Fig. 2(d), the controlled system of the

AC side is identified straightforward.

$$\begin{bmatrix} \dot{\tilde{i}}_1 \\ \dot{\tilde{i}}_2 \end{bmatrix} = \begin{bmatrix} -\frac{R_{AC}}{L_{AC}} & 0 \\ 0 & -\frac{R_{AC}}{L_{AC}} \end{bmatrix} \begin{bmatrix} \tilde{i}_1 \\ \tilde{i}_2 \end{bmatrix} + \begin{bmatrix} -\frac{1}{L_{AC}} & 0 \\ 0 & -\frac{1}{L_{AC}} \end{bmatrix} \left( \begin{bmatrix} u_\alpha \\ u_\beta \end{bmatrix} - \begin{bmatrix} v_{s,\alpha} \\ v_{s,\beta} \end{bmatrix} \right) \tag{2a}$$

$$= A_{AC,t}\tilde{i}_{AC,t} + B_{AC,t}\left(\underline{v}_t - \underline{z}_t\right) \tag{2b}$$

$$\begin{bmatrix} i_\alpha \\ i_\beta \end{bmatrix} = \begin{bmatrix} y_\alpha \\ y_\beta \end{bmatrix} = \begin{bmatrix} 2 & 0 \\ 0 & 2 \end{bmatrix} \begin{bmatrix} \tilde{i}_1 \\ \tilde{i}_2 \end{bmatrix} \tag{2c}$$

$$= C_{AC,t}\tilde{i}_{AC,t}. \tag{2d}$$

$R_{AC} = \tilde{R}_{5,6}$ and $L_{AC} = \tilde{L}_{5,6}$ are the effective system parameters towards the AC side. For the uncoupled MMC setup, they can be calculated to $R_{AC} = R + 2R_{ac}$ and $L_{AC} = L + 2L_{ac}$ $v_{s,\alpha}$ and $v_{s,\beta}$ are the transformed grid voltages. $\iota_\alpha$ and $\iota_\beta$ are the grid currents in $\alpha\beta$-representation.

For simplification those voltages are assumed to be fed forward ideally.

For implementation the voltage feed forward and phase locked loop (PLL) calculation is performed on an field programmable gate array (FPGA) to improve the system dynamics. A DSRF PLL is used in the stationary reference system [18–20]. The feedforward control of the measured AC voltage is performed directly on the FPGA with an increased modulation frequency of 40 kHz. The DSRF PLL is used to determine the positive sequence and negative sequence of the grid voltage in a reliable way. For energy pulsation reduction, an identification of the positive sequence current is mandatory [17]. $\tilde{i}_1$ and $\tilde{i}_2$ are the transformed currents to the AC side. $u_\alpha$ and $u_\beta$ are the input variables to control the currents. $y_\alpha$ and $y_\beta$ are the respective output currents.

For the purpose of this paper it is assumed, that the MMC energy control takes care of the safe operation of the system based on [11, 21]. This work focuses on the AC currents control of the system.

**Predictive Control Equations**

Starting from (2a) and (2d), the fundamental equations are derived. Since the control is computed in discret time on a DSP, the system equations $A_{AC,t}$, $B_{AC,t}$ and $C_{AC,t}$ must be transformed using the z-transform. Using the time-discrete state space matrices $A_{AC}$ and $B_{AC}$, the MPC can be implemented. The AC voltages of the grid appear as disturbance quantities on the system. They are separately fed forward and therefore do not have to be considered any further for the design of the current control system.

The idea then is to calculate the system evaluation for a given sequence of input variables $\tilde{U}(k) = \begin{bmatrix} \underline{v}_k & \underline{v}_{k+1} & \cdots & \underline{v}_N \end{bmatrix}^\top$ over the prediction horizon $N$, where $k$ denotes the actual time instance. This evaluation is subsequently solved for the optimal input sequence $\tilde{U}(k)$. The aim is to choose the $\tilde{U}(k)$ in a way, that the reference trajectories $y_{\text{ref},\alpha}$ and $y_{\text{ref},\beta}$ for the AC currents are sufficiently tracked.

For any given time $k+1$ the states can be calculated directly

$$\tilde{i}_{AC,k+l} = A_{AC}^l \tilde{i}_{AC,k} + \sum_{i=1}^{l} A_{AC}^{(l-i)} B_{AC}\underline{v}_{AC,(k+i-1)} \tag{3a}$$

Without restriction of the generality, the control is considered in this section with a prediction horizon of $N = 3$. The prediction horizon is one of the degrees of freedom in the design and performance of the model based control approach. The chosen value shows very good control results of the AC currents when implemented on the test system.

Using (2b) and (2d), the vector $\tilde{X}(k)$ and $\tilde{Y}(k)$ of the state and output variables and at time $k$ is calculated as

$$\tilde{X}(k) = \begin{bmatrix} \tilde{i}_{AC,1} & \tilde{i}_{AC,2} & \tilde{i}_{AC,3} \end{bmatrix}^\top \tag{4a}$$

$$\tilde{Y}(k) = \begin{bmatrix} \underline{y}_{AC,1} & \underline{y}_{AC,2} & \underline{y}_{AC,3} \end{bmatrix}^\top = \Gamma \tilde{i}_{AC,k} + \Upsilon \tilde{U}(k) \tag{4b}$$

with $\tilde{U}(k) = \begin{bmatrix} \underline{v}_{\text{AC},1} & \underline{v}_{\text{AC},2} & \underline{v}_{\text{AC},3} \end{bmatrix}^{\top}$. The system evaluation can be described using this approach.

To calculate the optimal input $\tilde{U}(k)$ for the next time steps, a cost function is required. The cost function must be optimized, i.e. minimized, within a control period of the system in order to satisfy the real-time condition.

The quadratic program (QP) represents a special form of optimization and is a good compromise between control result and calculation complexity [22]. In the QP, the cost function $J$ is a quadratic function with linear limiting functions. In the presented control approach, it is composed of a term $J_1$ and a term $J_2$. The first term formulates a quadratic quality measure for the deviation of the setpoint from the predicted value $\tilde{\xi}_{\text{AC},k} = \underline{y}^*_{\text{AC},k} - \underline{y}_{\text{AC},k}$. Not only the actual error is included in the calculation, but also the predicted deviations based on the model equations.

For this application $J_1$ and $J_2$ are chosen to

$$J_1 = \left\| \tilde{Y}(k)^* - \Gamma \underline{\tilde{i}}_{\text{AC},k} - \Upsilon \tilde{U}(k) \right\|^2_{\tilde{Q}} \tag{5a}$$

$$J_2 = \lambda_{\text{u}} \left\| S\tilde{U}(k) - E\underline{v}_{\text{AC},k-1} \right\|^2_2 \tag{5b}$$

$Q$ is the weighting matrix for the tracking error. To achieve a symmetrical weighting and thus symmetrical AC currents, the approach with the weighting factor $q_{\text{AC}}$ is $Q = q_{\text{AC}}I_2$ and

The second part $J_2$ of the cost function $J$ formulates a quality measure for the control effort. This means that the difference of the output variables between the time steps $\underline{v}_{\text{AC},k}$ and $\underline{v}_{\text{AC},k+1}$ is weighted and included in the total cost function. The weighting factor of the control effort is denoted by $\lambda_{\text{u}}$. Resulting in the matrices

$$\tilde{Q} = \begin{bmatrix} Q & 0 & 0 \\ 0 & Q & 0 \\ 0 & 0 & Q \end{bmatrix}; \quad S = \begin{bmatrix} I_2 & 0 & 0 \\ -I_2 & I_2 & 0 \\ 0 & -I_2 & I_2 \end{bmatrix}; \quad E = \begin{bmatrix} I_2 \\ 0 \\ 0 \end{bmatrix} \tag{6}$$

Here applies likewise, that an increase of the weighting factor $\lambda_{\text{u}}$ leads to an increase of the costs of the control effort. From the ratio of $q_{\text{AC}}$ and $\lambda_{\text{u}}$ the dynamics of the controller can be adjusted. This presented design results in a compromise between tracking accuracy of the setpoint trajectory and the required effort in regards to the output variables.

Using (5a) and (5b) the total cost function is calculated

$$J = J_1 + J_2 \tag{7a}$$

$$= \left\| \tilde{Y}(k)^* - \Gamma \underline{\tilde{i}}_{\text{AC},k} - \Upsilon \tilde{U}(k) \right\|^2_{\tilde{Q}} + \lambda_{\text{u}} \left\| S\tilde{U}(k) - E\underline{v}_{\text{AC},k-1} \right\|^2_2 \tag{7b}$$

$$= \dots \tag{}$$

$$= \tilde{U}(k)^{\top} H \tilde{U}(k) + 2\underline{\theta}_k^{\top} \tilde{U}(k) + \theta_k \tag{7c}$$

with

$$H = q_{\text{AC}} \Upsilon^{\top} \Upsilon + \lambda_{\text{u}} S^{\top} S \tag{7d}$$

$$\underline{\theta}_k = -\Upsilon^{\top} \tilde{Q} \left( \tilde{Y}(k)^* - \Gamma \underline{\tilde{i}}_{\text{AC},k} \right) - \lambda_{\text{u}} S^{\top} E \underline{v}_{\text{AC},k-1} \tag{7e}$$

The matrix $H$ is a time invariant matrix, depending on $A_{\text{AC}}$, $B_{\text{AC}}$, $C_{\text{AC}}$, $q_{\text{AC}}$ and $\lambda_{\text{u}}$. The dimension of $H$ is given by $H \in \mathbb{R}^{\dim(\underline{v}_{\text{AC},k}) \cdot N \times \dim(\underline{v}_{\text{AC},k}) \cdot N} = \mathbb{R}^{6 \times 6}$. Thereby is $H = H^{\top}$ and $H \succ 0$ (positive definite) for $\lambda_{\text{u}} > 0$. $\underline{\theta}_k$ is a time variant function of $\underline{\tilde{i}}_{\text{AC},k}$, the input variable of the preceding sampling interval $\underline{v}_{\text{AC},k-1}$, the setpoint trajectory $\tilde{Y}(k)^*$ as well as the weighting factors $\lambda_{\text{u}}$ and $q_{\text{AC}}$. The term $\theta_k$ is a time variant offset with $\theta_k \in \mathbb{R}$. Since $\theta_k$ does not depend on $\tilde{U}(k)$, it will vanish for all derivatives of $J$ with respect to $\tilde{U}(k)$. Therefore this term has no further influence on the minimization of the cost function. The

Table I: Technical specifications of the laboratory setup

| Parameter | Value | Parameter | Value |
|---|---|---|---|
| $P_{\text{MMC,N}}$ | 10 kW | $C_{\text{Cell}}$ | 6.6 mF |
| $V_{\text{dc}}$ | 650 V | $v_{\text{Cell}}$ | 150 V |
| $V_{\text{AC}}$ | 400 V | $f_{\text{C}}$ | 8 kHz |
| $\varphi_{\text{d}}$ | 0 to $2\pi$ | $f_{\text{M}}$ | 40 kHz |
| $I_{\text{branch,max}}$ | 40 A | $L_{\text{h,branch}}$ | 241 μH |
| $N_{\text{cell}}$ per branch | 5 | $L_{\sigma,\text{branch}}$ | 10.5 μH |
| semiconductors | IPP110N20N3 | $L_{\text{AC}}$ | 1.33 mH |
| $R_{\text{ds,on}}$ | 10.7 mΩ | $L_{\text{DC}}$ | 5.0 mH |

objective of the MPC is to find the minimum of the cost function $J$ from (7c) in dependence of the output variables $\tilde{U}(k)$ for each time step $k$.

This results in QP optimization problem which has to be solved under real time conditions. We take

$$\underset{\tilde{U}(k)}{\text{minimize}} \quad J = \tilde{U}(k)^\top H \tilde{U}(k) + 2\underline{\theta}_k^\top \tilde{U}(k) + \theta_k \tag{8a}$$

with the solution

$$\tilde{U}(k)^* = -H^{-1}\underline{\theta}_k. \tag{8b}$$

(8b) is the analytical, unconstrained solution for optimal input variables during the prediction horizont. $H$ is constant in time in this system and can therefore be inverted offline in advance. Subsequently, those input variables are limited. A limitation of the state variables is also possible, if the system is controlled in transformed quantities [23]. In addition, a compensation of a calculating time delay is added. Using this approach, an implementation on a laboratory setup is straightforward.

## Laboratory Setup

For verification, the algorithms are implemented on a signal processing system and tested on a real grid using a laboratory prototype. In the following section the concept of signal processing and the design of the prototype are presented. The setup is based on a laboratory prototype from [24]. The power section was modified and the signal processing was made more powerful. The signal processing is based on a System-On-Chip platform [25]. To ensure that the grid connection conditions are reproducible, an inverter-based island grid was developed [26]. This allows for the emulation of fixed grid conditions and the verification of control algorithms.

Table I lists the parameters of the built prototype. The MMC has a nominal power of $P_{\text{MMC,N}} = 10\,\text{kW}$. Each branch is a series circuit of $N = 5$ cells, with a maximum voltage of $v_{\text{C}} = 150\,\text{V}$. Coupled iron sheet arm inductors are used. Due to the very good coupling of the branch inductors, additional ferrite inductors are used as line inductors on the AC side.

Figures 3(a) to 3(c) show the laboratory setup of the MMC with power terminals and signal processing. Each of the 6 converter branches is realized on a pcb shown in Fig. 3(b). The MPC is implemented to be solved with a frequency of $f_{\text{MMC}} = 8\,\text{kHz}$. The PLL is calculated with $f_{\text{PLL}} = 40\,\text{kHz}$ on the FPGA directly.

## Measurement Results

In this section, measurement results obtained from the laboratory setup are presented. The modeling of the system and the derived control structures are verified and validated with the shown lab setup discussed. The implementation allows a real-time capable calculation of the constrained control algorithms.

(a) Lab setup of the MMC



(b) Branch PCB with 5 cells
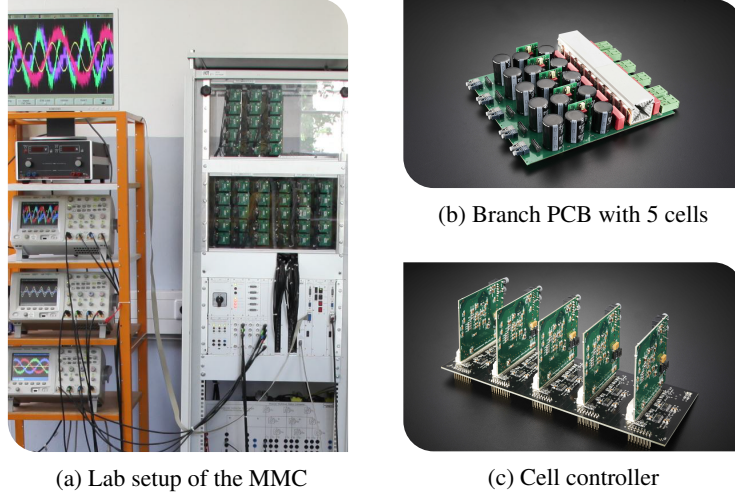


(c) Cell controller

Fig. 3: Laboratory setup with power section and signal processing of the laboratory prototype.

Quasi-stationary and dynamic measurements at the laboratory grid and the inverter-based island grid are presented to demonstrate the basic functionality of the control. Finally, the performance in case of a grid failure is shown.

First, a load step along the maximum voltage limit is presented. Second, the capability of the MPC in combination with the FPGA based PLL during a grid fault is shown. All measurements are sampled with the control system at a frequency of $f_s = 8\,\text{kHz}$.

## Quasi Stationary Operation of the System

The MMC is pre-charged and operated quasi-stationarily using the $400\,\text{V}/50\,\text{Hz}$ laboratory supply grid. The grid is connected via a Yz-transformer. Through this, the feeding network string voltage amplitude is $\hat{V}_{AC} = 400\,\text{V}/\sqrt{2} = 282\,\text{V}$. On the DC side, the MMC is controlled by a machine set with $V_{dc} = 450\,\text{V}$ The ratio is $V_{dc}/\hat{V}_{AC} \approx 1.6$. A power of $P = 8.5\,\text{kW}$ at a power factor of $\cos(\varphi_g) = 1$ is delivered to the AC grid.

Figures 4(a) and 4(b) show measurements of the grid voltages and grid currents in this operating point. As can be seen, the grid currents are precisely controlled stationarily by the predictive approach of AC control. Figure 4(c) depicts the measured arm currents of all 6 inverter arms. These are composed of a superposition of the AC currents and the DC current. In addition, currents are controlled to generate balancing power according to [23]. With 0.5 A these currents are small compared to the total arm current. The energy control is steady-state accurate and ensures stable operation of the system. Figure 4(d) shows the arm energies calculated from the measured arm voltages $v_{\text{arm}}$. The occurring energy pulsation is $\Delta W = 8.567\,\text{J}$. On average all energies are constant around the mean value $W_{\text{mean}} = 264.92\,\text{J}$, which corresponds to an arm voltage of $V_{\text{mean}} \approx 650\,\text{V}$.

The presented modelling and control approach is verified by implementation on a real-time laboratory setup.

### Dynamic Load Step at the AC Side

The new approach of predictive AC control allows a current increase along the voltage limit, without overshoot and with stationary accuracy.

The examination takes place in the transformed system, since the currents and output variables can be considered decoupled for the AC side. The maximum output variable for the AC side can be freely adjusted by decoupling the controlled system. To demonstrate the performance at the voltage limit, the maximum control voltage is set to $\tilde{u}_{AC,\text{max}} = \pm 50\,\text{V}$.

Figure 5(a) shows the transformed setpoints of the control variable to the time point of the load step. The limitation to $\pm 50\,\text{V}$ is clearly visible.
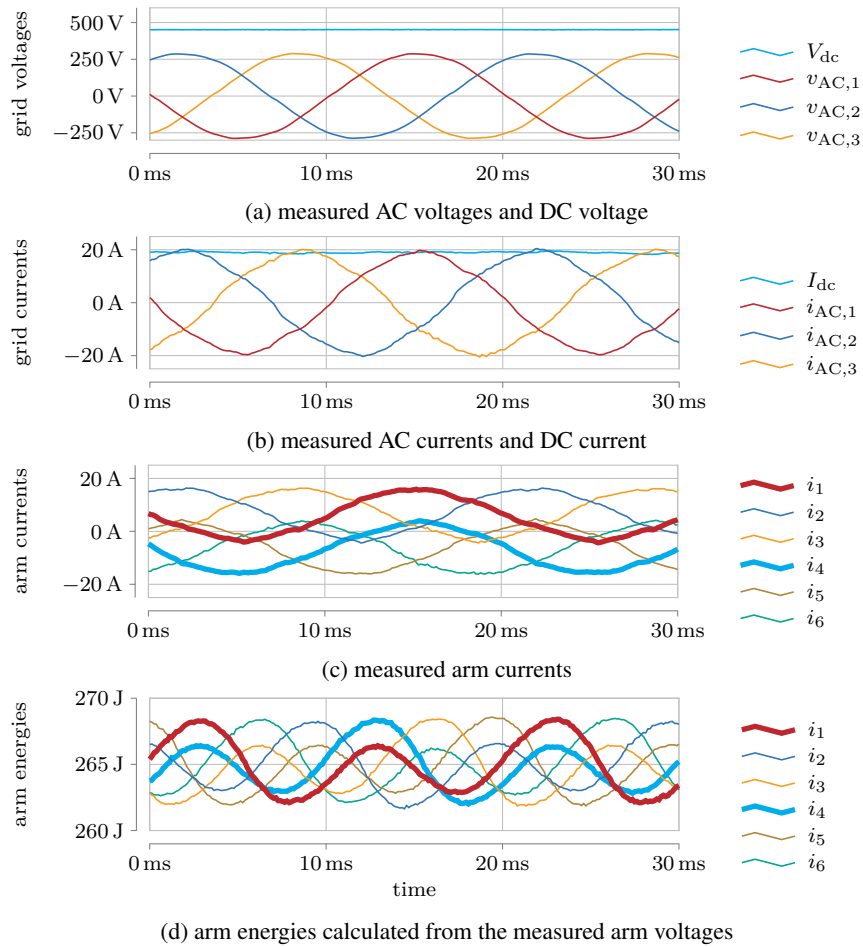
(a) measured AC voltages and DC voltage



(b) measured AC currents and DC current



(c) measured arm currents



(d) arm energies calculated from the measured arm voltages

Fig. 4: Quasi-stationary operation at the $400\,\text{V}/50\,\text{Hz}$-grid with $P = 8.5\,\text{kW}$. The measured values are sampled with the control period $T_\text{C} = 125\,\mu\text{s}$.

Figure 5(b) shows the transformed AC currents and their setpoints. By limiting the output variables, the current increases almost linearly until the setpoint is reached. Due to the modeling and the predictive approach the setpoint is reached with the greatest possible dynamics without overshoot and is precisely controlled in a steady-state manner.

**Stable Operation During Grid Faults**

In order to investigate the performance of the control system, it must be possible to set grid failures in a targeted and reproducible manner. Comparing the behavior of the compensation methods in a LVRT experiment requires that the grid voltage always drops by the same value at the same time. The island grid presented in [26] provides the basis for the test setup. A single phase voltage drop down to 20 % of the nominal voltage is emulated with the feeding MMC based converter to show the capability of the implemented MMC control.

Figures 6(a) to 6(c) show the measured values of the laboratory setup in case of a grid fault using different approaches to grid current handling. Before the grid fault, a constant AC power is delivered to the symmetrical, sinusoidal grid. At $t = 20\,\text{ms}$ the feeding converter emulates the grid error. Figure 6(a) shows the measured grid voltages. Before the grid fault, the currents are precisely controlled. In case of a fault, the PLL on the FPGA must continue to determine the grid angle exactly. Additionally, the negative sequence hast to be identified. This enables correct feedforward control of the voltage. During the transient compensation processes, the current in the line inductors increases because of the incorrect feedforward control. However, the AC side control is able to keep the current within the limits of $\pm 50\,\text{A}$ and thus avoids a fault state of the converters. Once the PLL correctly identifies all quantities, the current trajectories can be injected as sinusoidal three phase system (Fig. 6(b)) or in a manner that the AC power

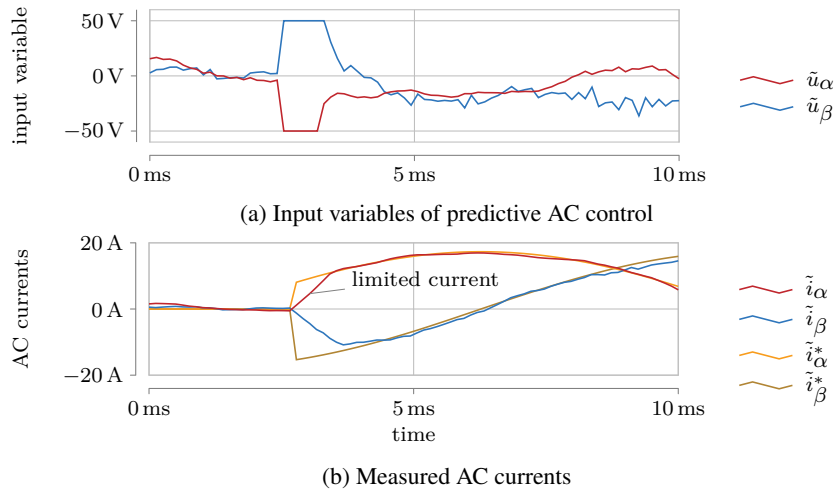(a) Input variables of predictive AC control



(b) Measured AC currents

Fig. 5: Constrained output variables and grid currents during a load step

stays constant after the grid fault (Fig. 6(c)).

The measurement results show that the modelling and control of the system allows a stable operation in case of a grid failure.

## Conclusion

In this paper an indirect model based predictive control for the grid currents of an MMC at $f_{\text{MMC}} = 8\,\text{kHz}$ is presented. The control is based on a decoupled consideration of the AC side. The modelling allows a very simple, real-time capable implementation on a laboratory prototype. Validation and measurements of the laboratory scale MMC on an inverter-based island grid show the dynamics of the current control. In addition, the fast implementation of the PLL allows to overcome grid errors and to feed constant power into the grid or keep the currents constant. The converter control is able to keep the capacitor voltages within their tolerance band. All this combined improves a dynamic, efficient and grid-compatible use of the MMC and enables it as tomorrow's backbone of the sustainable power supply.

## References

[1] A. Lesnicar and R. Marquardt, "An innovative modular multilevel converter topology suitable for a wide power range," in *IEEE Bologna PowerTech*, Piscataway, NJ: IEEE, 2003, pp. 272–277.

[2] Y. Pipelzadeh, B. Chaudhuri, T. Green, Y. Wu, H. Pang, and J. Cao, "Modelling and dynamic operation of the zhoushan dc grid: Worlds first five-terminal vsc-hvdc project," in *International High Voltage Direct Current*, Oct. 2015.

[3] S. Allebrod, R. Hamerski, and R. Marquardt, "New transformerless, scalable Modular Multilevel Converters for HVDC-transmission," in *IEEE Power Electronics Specialists Conference*, Piscataway, N.J.: IEEE, 2008, pp. 174–179.

[4] M. A. Perez, S. Bernet, J. Rodriguez, S. Kouro, and R. Lizana, "Circuit Topologies, Modeling, Control Schemes, and Applications of Modular Multilevel Converters," *IEEE Transactions on Power Electronics*, vol. 30, no. 1, pp. 4–17, 2015.

[5] S. Milovanovic, "MMC-based conversion for MVDC applications," Ph.D. dissertation, École polytechnique fédérale de Lausanne (EPFL), 2020.

[6] IEEE, "Proposed terms and definitions for flexible AC transmission system (FACTS)," *IEEE Transactions on Power Delivery*, vol. 12, no. 4, pp. 1848–1853, 1997.

[7] M. Pereira, D. Retzmann, J. Lottes, M. Wiesinger, and G. Wong, "SVC PLUS: An MMC STATCOM for network and grid access applications," in *IEEE Trondheim PowerTech*, IEEE, 2011, pp. 1–5.

[8] T. Nowak, M. Suriyah, and T. Leibfried, "Power tracking in a MMC-multi-terminal HVDC system with centralized and decentralized MPC using a black box modeling approach," in *52nd International Universities Power Engineering Conference (UPEC)*, I. U. P. E. Conference, Ed., IEEE, 2017, pp. 1–4.

[9] X. Jiang and M. M. Bakran, "Fault Current Behavior of MMC With the First Blocking Method," *IEEE Transactions on Power Electronics*, vol. 34, no. 12, pp. 11 616–11 628, 2019.

[10] P. Himmelmann and M. Hiller, "Solid-state transformer based on modular multilevel converters," *The Journal of Engineering*, vol. 17, pp. 4490–4494, 2019.

[11] J. Kolb, "Optimale Betriebsführung des Modularen Multilevel-Umrichters als Antriebsumrichter für Drehstrommaschinen," Ph.D. dissertation, Karlsruhe Institute of Technology (KIT), 2014.
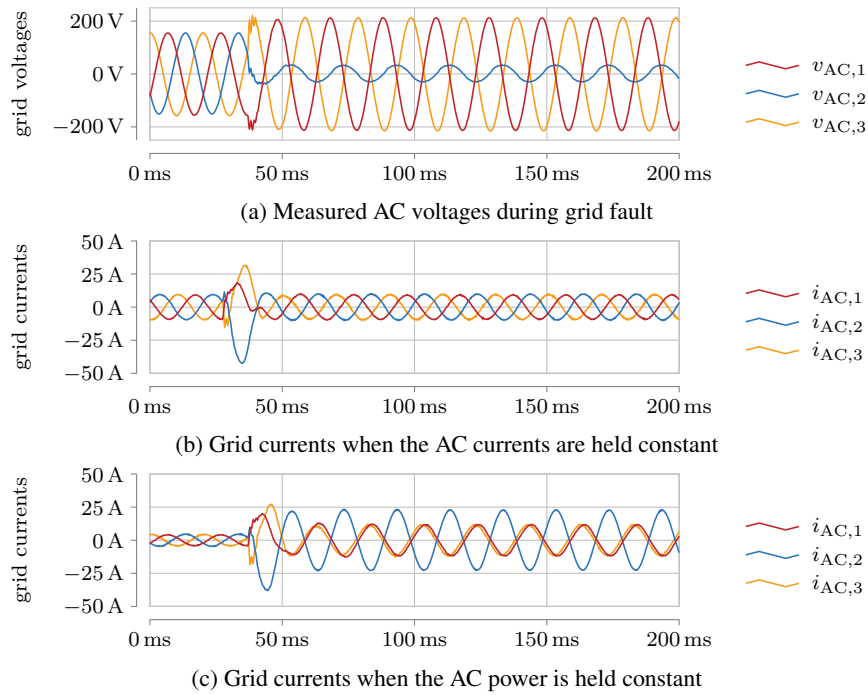
(a) Measured AC voltages during grid fault



(b) Grid currents when the AC currents are held constant



(c) Grid currents when the AC power is held constant

Fig. 6: Directly measured and derived variables during a grid fault with different approaches for fault handling.

[12] P. Himmelmann, M. Hiller, D. Krug, and M. Beuermann, "A new modular multilevel converter for medium voltage high power oil & gas motor drive applications," in *18th European Conference on Power Electronics and Applications (EPE'16 ECCE Europe)*, IEEE, 2016, pp. 1–11.

[13] T. Geyer, *Model predictive control of high power converters and industrial drives*, First edition. Chichester, West Sussex, United Kingdom: Wiley, 2017.

[14] J. Bocker, B. Freudenberg, A. The, and S. Dieckerhoff, "Experimental Comparison of Model Predictive Control and Cascaded Control of the Modular Multilevel Converter," *IEEE Transactions on Power Electronics*, vol. 30, no. 1, pp. 422–430, 2015.

[15] B. Gutierrez and S.-S. Kwak, "Modular Multilevel Converters (MMCs) Controlled by Model Predictive Control With Reduced Calculation Burden," *IEEE Transactions on Power Electronics*, vol. 33, no. 11, pp. 9176–9187, 2018.

[16] J. Qin and M. Saeedifard, "Predictive Control of a Modular Multilevel Converter for a Back-to-Back HVDC System," *IEEE Transactions on Power Delivery*, vol. 27, no. 3, pp. 1538–1547, 2012.

[17] D. Braeckle, P. Himmelmann, L. Gröll, V. Hagenmeyer, and M. Hiller, "Energy pulsation reduction in modular multilevel converters using optimized current trajectories," *IEEE Open Journal of Power Electronics*, vol. 2, pp. 171–186, 2021.

[18] F. Blaabjerg, R. Teodorescu, M. Liserre, and A. V. Timbus, "Overview of Control and Grid Synchronization for Distributed Power Generation Systems," *IEEE Transactions on Industrial Electronics*, vol. 53, no. 5, pp. 1398–1409, 2006.

[19] F. Blaabjerg, M. P. Kamierkowski, and R. Krishnan, *Control in power electronics: Selected problems*, ser. Academic Press series in engineering. Amsterdam and New York: Academic Press, 2002.

[20] R. Teodorescu, M. Liserre, and P. Rodríguez, *Grid converters for photovoltaic and wind power systems*. Chichester, West Sussey: Wiley IEEE, 2011.

[21] M. Hagiwara and H. Akagi, "PWM control and experiment of modular multilevel converters," in *IEEE Power Electronics Specialists Conference*, Piscataway, N.J.: IEEE, 2008, pp. 154–161.

[22] J. Nocedal and S. J. Wright, *Numerical Optimization*, Second Edition, ser. Springer Series in Operations Research and Financial Engineering. New York, NY: Springer Science+Business Media LLC, 2006.

[23] D. Bräckle, "under review: Contributions to Modelling and Control of Modular Multilevel Converter," Ph.D. dissertation, Karlsruhe Institute of Technology (KIT), 2021.

[24] F. Kammerer, "Systemanalyse und Regelung des Modularen Multilevel Matrix Umrichters als Antriebsumrichter," Ph.D. dissertation, Karlsruhe Institute of Technology (KIT), 2016.

[25] R. Schwendemann, S. Decker, M. Hiller, and M. Braun, *A Modular Converter- and Signal-Processing-Platform for Academic Research in the Field of Power Electronics*, 2018.

[26] D. Braeckle, S. Mersche, M. Schnarrenberger, P. Himmelmann, and M. Hiller, "Modular Multilevel Converters as Active Filters to Mitigate Low Frequency Current Harmonics in Converter Fed Grid Applications," in *PCIM Europe: International Exhibition and Conference for Power Electronics, Intelligent Motion, Renewable Energy and Energy Management*, 2018.